resonance imaging of 3660 elderly people: the Cardiovascular Health Study. *Arch Neurol* 1998; **55**: 1217–1225.
20 Vermeer SE, Den Heijer T, Koudstaal PJ, Oudkerk M, Hofman A, Breteler MM. Incidence and risk factors of silent brain infarcts in the population-based Rotterdam Scan Study. *Stroke* 2003; **34**: 392–396.
21 Araki Y, Nomura M, Tanaka H *et al.* MRI of the brain in diabetes mellitus. *Neuroradiology* 1994; **36**: 101–103.
22 den Heijer T, Vermeer SE, van Dijk EJ *et al.* Type 2 diabetes and atrophy of medial temporal lobe structures on brain MRI. *Diabetologia* 2003; **46**: 1604–1610.
23 Schmidt R, Launer LJ, Nilsson LG *et al.* Magnetic resonance imaging of the brain in diabetes: the Cardiovascular Determinants of Dementia (CASCADE) Study. *Diabetes* 2004; **53**: 687–692.
24 Minoshima S, Giordani B, Berent S, Frey KA, Foster NL, Kuhl DE. Metabolic reduction in the posterior cingulate cortex in very early Alzheimer's disease. *Ann Neurol* 1997; **42**: 85–94.
25 Mistur R, Mosconi L, Santi SD *et al.* Current Challenges for the Early Detection of Alzheimer's Disease: brain Imaging and CSF Studies. *J Clinl Neurol (Seoul, Korea)* 2009; **5**: 153–166.
26 Baker LD, Cross DJ, Minoshima S, Belongia D, Watson GS, Craft S. Insulin resistance and Alzheimer-like reductions in regional cerebral glucose metabolism for cognitively normal adults with prediabetes or early type 2 diabetes. *Arch Neurol* 2011; **68**: 51–57.
27 Furumoto S, Okamura N, Iwata R, Yanai K, Arai H, Kudo Y. Recent advances in the development of amyloid imaging agents. *Curr Top Med Chem* 2007; 7: 1773–1789.
28 Kudo Y, Okamura N, Furumoto S *et al.* 2-(2-[2-Dimethylaminothiazol-5-yl]ethenyl)-6- (2-[fluoro]ethoxy) benzoxazole: a novel PET agent for in vivo detection of dense amyloid plaques in Alzheimer's disease patients. *J Nucl Med* 2007; **48**: 553–561.
29 Okamura N, Fodero-Tavoletti MT, Kudo Y *et al.* Advances in molecular imaging for the diagnosis of dementia. *Expert Opin Med Diagn* 2009; **3**: 705–716.
30 Arai H, Okamura N, Furukawa K, Kudo Y. Geriatric medicine, Japanese Alzheimer's disease neuroimaging initiative and biomarker development. *Tohoku J Exp Med* 2010; **221**: 87–95.
31 Furukawa K, Okamura N, Tashiro M *et al.* Amyloid PET in mild cognitive impairment and Alzheimer's disease with BF-227: comparison to FDG-PET. *J Neurol* 2010; **257**: 721–727.
32 McKhann G, Drachman D, Folstein M, Katzman R, Price D, Stadlan EM. Clinical diagnosis of Alzheimer's disease: report of the NINCDS-ADRDA Work Group under the auspices of Department of Health and Human Services Task Force on Alzheimer's Disease. *Neurology* 1984; **34**: 939–944.
33 Matsui T, Higuchi M, Okamura N, Arai H, Sasaki H. A practical method to predict rate of cognitive decline in mild to moderate Alzheimer's disease. *Neurology* 1999; **53**: 2208–2209.
34 Fazekas F, Kleinert R, Offenbacher H *et al.* Pathologic correlates of incidental MRI white matter signal hyperintensities. *Neurology* 1993; **43**: 1683–1689.
35 Zhao WQ, De Felice FG, Fernandez S *et al.* Amyloid beta oligomers induce impairment of neuronal insulin receptors. *FASEB J* 2008; **22**: 246–260.

ELSEVIER

Neurobiology of Aging 33 (2012) 2321–2323

NEUROBIOLOGY OF AGING

www.elsevier.com/locate/neuaging

Glucose metabolism and gray-matter concentration in apolipoprotein E ε4 positive normal subjects

Miharu Samuraki[a,*], Ichiro Matsunari[b], Wei-Ping Chen[b], Keisuke Shima[a], Daisuke Yanase[a], Nozomi Takeda[b], Hiroshi Matsuda[c], Masahito Yamada[a]

[a] *Department of Neurology and Neurobiology of Aging, Kanazawa University Graduate School of Medical Science, Kanazawa-city, Ishikawa, Japan*
[b] *The Medical and Pharmacological Research Center Foundation, Hakui-city, Ishikawa, Japan*
[c] *Department of Nuclear Medicine, Saitama Medical University International Medical Center, Hidaka-city, Saitama, Japan*

Received 3 Nov 2010; received in revised form 10 Nov 2011; accepted 12 Nov 2011

Abstract

Apolipoprotein E (ApoE) ε4 is known as a genetic risk factor for Alzheimer's disease (AD). This study investigated the prevalence of imaging abnormalities suggestive of AD in cognitively normal ApoE ε4 carriers using ^{18}F-fluorodeoxyglucose (FDG) positron emission tomography (PET) and voxel-based morphometry (VBM). Forty-five cognitive normal ApoE ε4 allele carriers and 45 noncarriers underwent both FDG positron emission tomography and magnetic resonance imaging (MRI). A total of 90 normal database sets were generated for the individual 45 ε4 carriers and 45 noncarriers. Mean *z*-scores in the predefined AD-specific regions of interest (ROI) were calculated for each ε4 carrier and noncarrier using the individually defined normal database. The prevalence of AD-like hypometabolism and atrophy in the ε4 carriers was 8.9% and 17.7%, respectively, and did not differ significantly from those in the noncarriers (8.9%, 8.8%). The majority of ε4 carriers showed preserved FDG uptake or gray matter concentration.

Keywords: Alzheimer's disease; FDG PET; ApoE ε4

1. Introduction

There is general agreement that the apolipoprotein E (ApoE) ε4 is a genetic risk factor for developing Alzheimer's disease (AD). The ApoE ε4 allele has been associated with glucose metabolic activity impairment even in cognitively normal subjects (Langbaum et al., 2010; Reiman et al., 1996), although conflicting results still exist as to whether loss of gray matter truly occurs in ε4 carriers (Lemaître et al., 2005; Reiman et al., 1998). The aim of this study was to investigate the prevalence of AD-like imaging abnormalities in cognitively healthy ApoE ε4 carriers using ^{18}F-fluorodeoxyglucose (FDG) positron emission tomography (PET) and structural magnetic resonance imaging (MRI) by using a voxel-based method.

2. Methods

We identified 112 ε4 carriers and 410 ε4 noncarriers from a total of 535 subjects (289 males, 246 females; age range, 23–81 years; mean age, 50.16 ± 15.36 years). From the 112 ε4 carriers, 45 carriers were randomly selected, and from 410 noncarriers, 45 noncarriers were selected matching for age, gender, education level, and score of Mini Mental State Examination (MMSE) to the 45 carriers (Supplementary Table 1).

All subjects underwent both FDG PET and MRI. A total of 90 normal database sets (each consisting of 20 noncarriers matched for age, gender, and education level) were generated for the individual 45 ε4 carriers and 45 noncarriers. The detailed procedures for image processing were

* Corresponding author at: Department of Neurology and Neurobiology of Aging, Kanazawa University, Graduate School of Medical Science, 13–1, Takara-town, Kanazawa-city, Ishikawa 920-8640, Japan. Tel.: +81 76 265 2292; fax: +81 76 234 4253.
E-mail address: kimiharu@med.kanazawa-u.ac.jp (M. Samuraki).

0197-4580/$ – see front matter © 2012 Elsevier Inc. All rights reserved.
10.1016/j.neurobiolaging.2011.11.020

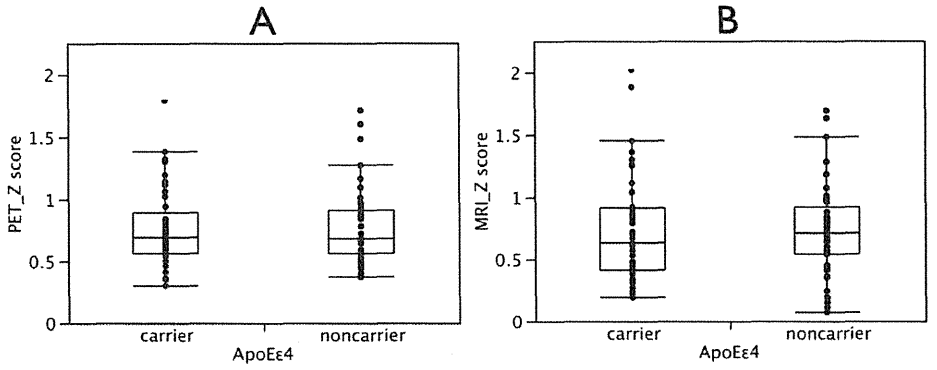

Fig. 1. Box-and-whisker plots of mean z-score in the Alzheimer's disease (AD)-specific region of interest (ROI) on fluorodeoxyglucose-positron emission tomography (FDG PET) (A) and magnetic resonance (MR) image (B) in apolipoprotein E (ApoE) ε4 carrier group and noncarrier group.

described in Supplementary data. In brief, all PET images were spatially normalized to a standardized stereotactic space in a same manner as our previous study (Matsunari et al., 2007) using an FDG PET template that had been constructed by averaging FDG images of 27 AD and 40 normal subjects (Matsunari et al., 2007). The optimized voxel-based morphometry (VBM) was performed for all magnetic resonance (MR) images in a manner as described by Good et al. (2001). We used the custom T1 template and prior gray or white matter and cerebrospinal fluid templates generated from the same subjects who had been used for FDG PET template.

Mean z-scores in the predefined AD-specific regions of interest (ROI) (Matsunari et al., 2007) were calculated for each ε4 carrier and noncarrier using the individually defined normal database, and the prevalence of the subjects who presented AD-like glucose hypometabolism and/or atrophy with high z-score was compared between the ε4 carrier group and the noncarrier group.

3. Results

The subjects with significant increases of mean z-score in the FDG PET ROI were 4 in the carriers, and 4 in the noncarriers, and the prevalence was 8.9% in the carriers, and 8.9% in the noncarriers. The average mean z-score in the ROI of the 45 ε4 carriers was 0.76 ± 0.31, and that of the 45 noncarriers was 0.78 ± 0.30. No significant differences were revealed between carriers and noncarriers ($p = 0.8055$) (Fig. 1A).

The subjects with significant increases of mean z-score in the MRI ROI were 8 in the carriers and 4 in the noncarriers, and the prevalence was 17.7% in the carriers and 8.9% in the noncarriers. Although the prevalence of carriers with reduced gray matter concentration was slightly higher, there were no statistical differences between the 2 groups ($p = 0.2148$, Pearson χ^2 test). The average mean z-score in the ROI of 45 ε4 carriers was 0.73 ± 0.42, and that of 45 noncarriers was 0.73 ± 0.36. There was also no significant difference between the 2 groups ($p = 0.6455$) (Fig. 1B).

4. Discussion

Several studies have reported that cognitive normal ApoE ε4 carriers show glucose hypometabolism in posterior cigulate gyri, precuneus, parieto-temporal lobes, and prefrontal regions suggestive of AD (Reiman et al., 1996). Regarding MRI, Reiman et al. (1998) reported insignificant changes of hippocampal volumes in normal ε4 carriers. They hypothesized that glucose metabolism begins to decrease before hippocampal atrophy begins in normal ε4 carriers (Reiman et al., 1998). On the other hand, other studies reported that ε4 homozygous carriers show significant decrease of gray matter in medial temporal lobe compared with the heterozygous carriers and noncarriers (Lemaître et al., 2005). Thus, though ApoE ε4 has been considered to have relevance to metabolic and morphological abnormalities since the preclinical AD stage, there is no consensus as to what extent ApoE ε4 has an effect upon those images. Additionally, there are no studies revealing the direct effect of ApoE on metabolic change, and the possibility remains that ApoE indirectly affects AD onset and progression by modulating the function of cerebrovascular system (Kim et al., 2009). Thus, from the point of the mechanism, influences of ApoE on brain metabolism are also still obscure.

The previous studies performed group-comparison between normal ε4 carriers and noncarriers, and could not reveal the prevalence of image abnormalities suggestive of AD in normal carriers and noncarriers. Additionally, almost all of those studies were case-controlled studies with targets limited to normal controls with family history of AD, relatively narrow age range, and high education level. On the other hand, this study did not limit subjects related to age or family history, and the sample size was relatively large. This study could reveal a relatively low prevalence of FDG PET and MRI changes

suggestive of AD in normal ε4 carriers and in noncarriers using 1 by 1 comparison.

These results indicated that the effect of ApoE ε4 allele alone on FDG uptake and gray matter concentration of normal subjects would be slight in volunteer-based populations and the possibility that other factors affect those images.

4.1. Study limitation

The use of age-specific normal database, despite necessary to avoid potential age-related effects on Z-score maps, may potentially lead to Z maps which could not be reliably compared one to the other. However, additional analyses using a single age-composite database confirmed the main findings of the current study (data not shown), showing its robustness to the normal used.

Additionally, because we had to keep our data processing technique strictly similar to that used in our previous publication, it was not optimized. It is thus possible that an updated/more refined methodology would allow detection of more subtle changes (i.e., a higher proportion of AD-like changes within the carriers).

Appendix A. Supplementary data

Supplementary data associated with this article can be found, in the online version, at doi:10.1016/j.neurobiolaging.2011.11.020.

References

Good, C.D., Johnsrude, I.S., Ashburner, J., Henson, R.N., Friston, K.J., Frackowiak, R.S., 2001. A voxel-based morphometric study of ageing in 465 normal adult human brains. Neuroimage 14, 21–36.

Kim, J., Basak, J.M., Holtzman, D.M., 2009. The role of apolipoprotein E in Alzheimer's disease. Neuron 63, 287–303.

Langbaum, J.B., Chen, K., Caselli, R.J., Lee, W., Reschke, C., Bandy, D., Alexander, G.E., Burns, C.M., Kaszniak, A.W., Reeder, S.A., Corneveaux, J.J., Allen, A.N., Pruzin, J., Huentelman, M.J., Fleisher, A.S., Reiman, E.M., 2010. Hypometabolism in Alzheimer-affected brain regions in cognitively healthy Latino individuals carrying the apolipoprotein E epsilon4 allele. Arch. Neurol. 67, 462–468.

Lemaître, H., Crivello, F., Dufouil, C., Grassiot, B., Tzourio, C., Alpérovitch, A., Mazoyer, B., 2005. No epsilon4 gene dose effect on hippocampal atrophy in a large MRI database of healthy elderly subjects. Neuroimage 24, 1205–1213.

Matsunari, I., Samuraki, M., Chen, W.P., Yanase, D., Takeda, N., Ono, K., Yoshita, M., Matsuda, H., Yamada, M., Kinuya, S., 2007. Comparison of 18F-FDG PET and Optimized Voxel-Based Morphometry for Detection of Alzheimer's Disease: Aging Effect on Diagnostic Performance. J. Nucl. Med. 48, 1961–1970.

Reiman, E.M., Caselli, R.J., Yun, L.S., Chen, K., Bandy, D., Minoshima, S., Thibodeau, S.N., Osborne, D., 1996. Preclinical evidence of Alzheimer's disease in persons homozygous for the epsilon 4 allele for apolipoprotein E. N Engl J. Med. 334, 752–758.

Reiman, E.M., Uecker, A., Caselli, R.J., Lewis, S., Bandy, D., de Leon, M.J., De Santi, S., Convit, A., Osborne, D., Weaver, A., Thibodeau, S.N., 1998. Hippocampal volumes in cognitively normal persons at genetic risk for Alzheimer's disease. Ann. Neurol. 44, 288–291.

ELSEVIER

Neurobiology of Aging 33 (2012) 2006–2017

NEUROBIOLOGY OF AGING

www.elsevier.com/locate/neuaging

Posterior cingulate atrophy and metabolic decline in early stage Alzheimer's disease

Keisuke Shima[a], Ichiro Matsunari[b,*], Miharu Samuraki[a], Wei-Ping Chen[b], Daisuke Yanase[a], Moeko Noguchi-Shinohara[a], Nozomi Takeda[b], Kenjiro Ono[a], Mitsuhiro Yoshita[a], Yoshiharu Miyazaki[b], Hiroshi Matsuda[c], Masahito Yamada[a]

[a] *Department of Neurology and Neurobiology of Aging, Kanazawa University, Graduate School of Medical Science, Kanazawa, Japan*
[b] *Department of Clinical Research, the Medical and Pharmacological Research Center Foundation, Hakui, Japan*
[c] *Department of Nuclear Medicine, Saitama Medical University International Medical Center, Saitama, Japan*

Received 17 May 2010; received in revised form 23 June 2011; accepted 12 July 2011

Abstract

To test the hypothesis that Alzheimer's disease (AD) patients with posterior cingulate/precuneus (PCP) atrophy would be a distinct disease form in view of metabolic decline. Eighty-one AD patients underwent ^{18}F-fluorodeoxyglucose (FDG) positron emission tomography (PET) and structural magnetic resonance imaging (MRI). Positron emission tomography and voxel-based morphometry (VBM) Z-score maps were generated for the individual patients using age-specific normal databases. The patients were classified into 3 groups based on atrophic patterns (no-Hipp-PCP, atrophy in neither hippocampus nor PCP; Hipp, hippocampal atrophy; PCP, PCP atrophy). There were 16 patients classified as no-Hipp-PCP, 55 as Hipp, and 10 as PCP. The Mini Mental State Examination (MMSE) score was similar among the groups. The greater FDG decline than atrophy was observed in all groups, including the no-Hipp-PCP. The PCP group was younger, and was associated with a greater degree of FDG decline in PCP than the others. There are diverse atrophic patterns in a spectrum of AD. In particular, a subset of patients show PCP atrophy, which is associated with greater metabolic burden.

Keywords: Alzheimer's disease; Atrophy; Neuroimaging; Cerebrospinal fluid

1. Introduction

Alzheimer's disease (AD) is the leading form of age-related dementia in many countries and therefore, efforts have been made to characterize its pathophysiology using noninvasive or invasive biomarkers such as neuroimaging (Petrella et al., 2003) or tau-protein in cerebrospinal fluid (CSF) (Marksteiner et al., 2007). Of these, structural magnetic resonance imaging (MRI) has attracted great attention because it is noninvasive and relatively widely available in clinical settings. Prior studies have demonstrated that atrophy of the medial temporal lobe, including the hippocampal area, is a common structural feature of AD (Petrella et al., 2003). However, recent studies using structural MRI combined with the voxel-based morphometric (VBM) approach have demonstrated that diverse atrophic patterns may exist in a spectrum of AD (Frisoni et al., 2007). Some structural MRI studies have demonstrated that AD-associated brain atrophy may involve not only the medial temporal lobe but also the posterior cingulate gyri/precuneus (PCP), and parietotemporal area particularly in early onset AD (Ishii et al., 2005a; Shiino et al., 2006). These brain structures are known to be the area where AD-associated metabolic reduction occurs even at early stage as assessed by positron emission tomography (PET) with ^{18}F-fluorodeoxyglucose (FDG) (Herholz et al., 2002; Minoshima et al., 1997; Petrella et al., 2003). It is also noteworthy that AD patients with posterior cortical atrophy reportedly reveal greater

* Corresponding author at: The Medical and Pharmacological Research Center Foundation, Wo 32, Inoyama, Hakui, Ishikawa, 925-0613, Japan. Tel.: +81 767 26 3311; fax: +81 767 26 3314.
E-mail address: matsunari@mprcf.or.jp (I. Matsunari).

0197-4580/$ – see front matter © 2012 Elsevier Inc. All rights reserved.
10.1016/j.neurobiolaging.2011.07.009

neurofibrillary tangle (NFT) densities in the neocortical areas than in the hippocampal areas (Tang-Wai et al., 2004), suggesting the presence of a distinct form of AD mainly involving the neocortex. To date, however, the relationship between such atrophic patterns and metabolic disease extent/severity assessed by FDG PET is unknown.

The CSF biomarkers, on the other hand, are considered to reflect ongoing histopathological changes in the brain. It is known that AD is associated with elevated phosphorylated tau (p-tau) or reduced amyloid-beta (Aβ) 42 protein (Marksteiner et al., 2007). In particular, high tau levels have often been associated with a more rapid decline of cognitive function (Snider et al., 2009), and higher NFT densities (Tapiola et al., 1997), suggesting that CSF biomarkers may reflect disease aggressiveness. The levels of CSF biomarkers have also been linked to cognitive profiles (Koric et al., 2010; van der Vlies et al., 2009). Thus, CSF biomarkers may be of important value not only for diagnosis but for disease characterization. However, data on the relationship among CSF biomarkers, brain atrophic patterns, and cognitive profiles are missing.

The aim of this study was to test the hypothesis that AD patients with PCP atrophy would represent a distinct disease form associated with a greater metabolic decline, and more increased CSF p-tau levels, which may be linked to disease aggressiveness. In this study, we computed the VBM and PET *Z*-score maps (Chételat et al., 2008) using age-specific normal database sets strictly matched to each individual AD patient in order to avoid confounding aging effects on the resulting *Z*-score maps. Furthermore, we applied correction for partial-volume effects (PVE) on PET to compensate for atrophy in small brain structures.

2. Methods

This study was performed as a part of the Ishikawa Brain Imaging Study (IBIS) (initiated in 2002) to investigate the role of brain imaging using PET and MRI for early and objective assessment of AD and other forms of neurodegerative diseases, and the study protocol was approved by the institutional ethical committee and written informed consent was obtained from all subjects before the participation in the study.

2.1. Patients

We recruited 81 consecutive right-handed patients with clinical diagnosis of probable AD (41 men and 40 women; age range, 47–79 years; mean age ± SD, 69 ± 8 years) at mild stage. All patients were examined by neurologists at an academic memory disorders clinic. The inclusion criteria were: (1) diagnosis of probable AD according to the National Institute of Neurological and Communicative Disorders and Stroke and the Alzheimer's Disease and Related Disorders Association criteria (NINCDS-ADRDA) (McKhann et al., 1984); (2) no evidence of focal brain lesions on magnetic resonance (MR) images; and (3) mild functional severity: grades 0.5 or 1 on Clinical Dementia Rating (CDR) (Hughes et al., 1982). Patients with CDR 0.5 were included if they later progressed to fulfill the AD criteria. We excluded patients with complications from other neurological disease or an unwell physical condition, or with presence of severe language, attention, and/or behavioral disorders that would make the imaging procedure difficult. The mean Mini Mental State Examination (MMSE) score of the patients was 22.7 ± 3.2. Additionally, early- or late-onset AD patients were defined as those with age of disease onset earlier or later than 65 years.

2.2. Neuropsychological tests

In addition to MMSE described above, general intelligence was assessed using the Japanese translation of the Wechsler Adult Intelligence Scale-Revised (WAIS-R) (Wechsler, 1981). Furthermore, cognitive profile was assessed using the Japanese translation of the Wechsler Memory Scale-Revised (WMS-R) (Wechsler, 1987). The WAIS-R scores were evaluated in full-scale IQ, verbal IQ, and performance IQ; the WMS-R scores in 5 domains (verbal memory, visual memory, general memory, attention/concentration, and delayed recall).

2.3. Subjects for age-specific normal databases

In order to avoid age-related effects on the VBM or PET *Z*-score maps, we generated age-specific normal databases from a pool of 782 volunteers (402 men and 380 women, mean age 56.3 ± 16.3 years) recruited in response to advertisement. Each database consisted of 20 right-handed healthy subjects (10 men and 10 women), and was strictly matched for age (all subjects in each database were required to be within 5 years of the target age, and the difference between the mean age of database and target was kept < 1 year) to the individual AD patients. The number of 20 subjects for each normal database was determined based on our prior study demonstrating that the inclusion of 20 subjects is preferable for generating a normal database (Chen et al., 2008). The criteria to define "healthy" were: (1) no history of significant brain head trauma, psychiatric, or neurological disorders, uncontrolled major systemic diseases, and current use of centrally acting drugs; (2) no abnormalities on general and neurological examination' (3) MMSE score of 28 or higher and no clinical evidence of dementia; and (4) T2-weighted MRI or MR angiography detected no asymptomatic cerebral infarction or brain vessel abnormalities. The 81 AD patients fell into 27 age categories (e.g., 47 years, 49 years, 53 years, etc). Accordingly, a total of 27 age-specific normal database sets were generated using 267 healthy subjects (130 men and 137 women, mean age of 62 ± 9 years, mean MMSE score of 29.4 ± 0.7).

Additionally, we recruited 30 healthy subjects (13 men and 17 women, mean age 65.0 ± 6.0 years, mean MMSE score of 29.6 ± 0.6) from a pool of 130 volunteers, which is a

separate population from that used for generating normal databases, to determine normal VBM and PET Z-score values.

2.4. Imaging protocol

Both FDG PET and structural MRI were performed on the same day in both AD patients and healthy subjects. The detailed imaging procedure is described elsewhere (Samuraki et al., 2007). In brief, MR studies were performed using a 1.5 Tesla system (Signa Horizon, General Electric Medical Systems, Milwaukee, WI, USA). A 3-dimensional volumetric acquisition of a T1-weighted gradient echo sequence produced a gapless series of thin transaxial sections using a magnetization preparation rapid acquisition gradient-echo sequence (echo time/repetition time, 2.0/9.2 ms; flip angle, 20°; acquisition matrix, 256 × 192; number of slices, 124; pixel size, 0.78 × 1.04; slice thickness, 1.4 mm).

The subjects fasted for at least 4 hours prior to PET scanning. Before PET was performed, an intravenous line was established in all subjects. Each subject was placed supine on a bed. The subject's eyes were closed and covered with a mask; the ears were unoccluded, and the background noise was kept at a minimal level. Twenty minutes later, 370 MBq of ^{18}F-FDG was injected intravenously and subjects were kept in resting condition for an additional 40 minutes, then PET imaging was initiated for 10 minutes in 2-D mode. Transmission scan was carried out for 10 minutes using rotating ^{68}Ge pin sources. PET imaging was performed using a full-ring PET scanner (Advance, General Electric Medical Systems, Milwaukee, WI, USA). Images were reconstructed using an ordered-subset expectation-maximization algorithm. The image data matrix was 128 × 128 with a pixel size of 2.11 mm and a slice thickness of 4.25 mm. Both attenuation and scatter corrections were employed during image reconstruction.

2.5. PVE *correction for* FDG PET

To avoid the effects of brain atrophy on measured FDG activity, PVE-corrected FDG PET was obtained for both AD patients and healthy subjects in a manner as previously described (Matsuda et al., 2003; Yanase et al., 2005). In brief, an original PET image was coregistered to MRI after scalp editing of an original MR image using a binary mask for whole brain. The original MRI was segmented into white matter, gray matter, and CSF. Segmented images were convoluted with the point spread function of the PET device. A white matter PET image was then simulated from the convoluted white matter MR image. For this simulation, the region of interest (ROI) was automatically determined by setting the threshold to > 99% of the maximum count density of white matter MR images and the maximum count for white matter of PET was obtained. Gray matter PET images were obtained by subtraction of the simulated white matter PET images from the original PET image coregistered to MRI. Lastly, the gray matter PET image was divided by the convoluted gray matter MR image on a voxel-by-voxel basis. A gray matter PVE-corrected PET image was finally obtained by the application of a binary mask for gray matter to the divided image. Each step of the PVE correction algorithm was carefully checked by visual inspection to confirm that each step had been appropriately processed.

2.6. Image processing and analysis

The original T-1 weighted MR images were spatially normalized using SPM5 (Statistical Parametric Mapping, Wellcome Department of Cognitive Neurology, London, UK; www.fil.ion.ucl.ac.uk/spm) running on Matlab 7.6 (The MathWorks, Natick, MA, USA) to a standardized stereotactic space based on the Montreal Neurological Institute, using 12-parameter linear affine normalization and further 12 nonlinear iteration algorithms. The gray matter PET images were spatially normalized using the same parameters that were used for normalization of MR images. The PVE-corrected PET images were then smoothed using a 12-mm full-width at half-maximum (FWHM) isotropic Gaussian kernel. Proportional scaling was used to achieve global normalization of voxel values between images.

2.7. Voxel-based morphometry

Regional gray matter atrophy was assessed using optimized VBM that has been described by Good et al. (2001). The gray/white matter images segmented from original MR images were spatially normalized using gray/white matter templates. Then, the normalization parameters were applied to the original MR images. The normalized whole brain images were segmented into gray and white matter, CSF, and non-CSF partitions. Each optimally normalized and segmented gray matter image was smoothed with a 12-mm full-width at half-maximum kernel.

2.8. Tomographic Z-score mapping

After preprocessing of FDG PET and MRI data using SPM5 (Wellcome Department of Cognitive Neurology) as described above, each FDG PET or gray matter image of individual AD patients was compared with the mean and SD of FDG PET or gray matter images of the age-specific normal database using voxel-by-voxel Z-score analysis using a software program developed by Matsuda et al. (Matsuda, 2007); Z-score = ([control mean]−[individual value])/(control SD). These Z-score maps were displayed by overlay on tomographic sections. In each Z-score map, WFU Pickatlas (Department of Radiology of Wake Forest University School of Medicine, Winston-Salem, NC; fmri.wfubmc.edu) (Maldjian et al., 2003; Tzourio-Mazoyer et al., 2002) -based ROIs were drawn on the hippocampus, posterior cingulate/precuneus, frontal lobe, occipital lobe, parietal lobe, and temporal lobe. Using the averaged value of positive Z-scores in the hippocampus and posterior cingulate/precuneus ROIs, the AD patients were divided into 3 groups: (1) no-Hipp-PCP, no significant atrophy (Z-score of < 1.0) in hippocampus or

posterior cingulate/precuneus; (2) Hipp, hippocampal Z-score ≥ 1.0 and hippocampal Z-score > posterior cingulate/precuneus Z-score; and (3) PCP, posterior cingulate/precuneus Z-score ≥ 1.0 and posterior cingulate/precuneus Z-score > hippocampal Z-score. In order to investigate further the relationship between atrophy and metabolic decline, the AD patients were also divided into 3 groups based on FDG PET Z-score maps (PET-no-Hipp-PCP, PET-Hipp, and PET-PCP) using the same criteria as those used for VBM.

2.9. *APOE typing, CSF sampling, and analysis*

Venous blood samples were obtained in 67 patients for apolipoprotein E (APOE) phenotyping. The phenotype was determined by isoelectric focusing/immunoblotting using serum samples, as described by Kataoka et al. (1994). CSF was obtained in 52 patients by lumbar puncture to analyze p-tau, and Aβ42. For measurement of Aβ42, CSF and plasma samples were kept frozen until the analysis. Sandwich enzyme-linked immunosorbent assay (ELISA) was used to measure CSF Aβ42 (Innotest β-amyloid (1–42), Innogenetics, Ghent, Belgium), and CSF p-tau (Innotest Phosphotau (181p); Innogenetics) as described previously (Matsumoto et al., 2007). The CSF-p-tau was measured by detecting an epitope of the phosphorylated form of amino acid 181 in the tau protein. The cutoff values for normal p-tau and Aβ42 in our laboratory were 49 pg/mL and 490 pg/mL, respectively (Morinaga et al., 2010).

2.10. *Statistical analysis*

Data were expressed as mean ± SD. Statistical analysis was performed using JMP8 (SAS Institute, Inc. Cary, NC, USA), GraphPad Prism5 (GraphPad Software, Inc. San Diego, CA), or SPSS18 (SPSS, Inc. Chicago, IL, USA), where appropriate. Comparisons of mean values were performed using analysis of variance (ANOVA) and Tukey's multiple comparisons test unless specified. Analysis of covariance (ANCOVA) was used to compare mean values adjusted for age. Welch analysis of variance testing was used when the variances were unequal by Bartlett's test. The Z-score values among the patient groups were compared using Kruskal-Wallis test and Dunn's multiple comparisons test. Paired Z-score values between VBM and FDG PET were compared using Wilcoxon sign rank test. These nonparametric methods were used because of skewness in the imaging data. Linear regression was performed by least squares analysis. Proportional difference among the groups was assessed using χ^2 test or Fisher's exact test, where appropriate. Statistical significance was defined as $p < 0.05$.

3. Results

3.1. *Voxel-based morphometry, clinical characteristics, and CSF biomarkers*

Fig. 1 depicts the relationship of regional gray matter concentration loss between the hippocampus and posterior cingulate/precuneus plotted separately for early- (n = 23) and late-onset (n = 58) AD. There was no overall correlation of the degree of atrophy between the hippocampus and PCP (R = 0.082, not significant). Based on Z-score value in the hippocampus and posterior cingulate/precuneus, 16 AD patients (20%) were classified as no-Hipp-PCP (significant atrophy in neither hippocampus nor posterior cingulate/precuneus), 55 (68%) as Hipp dominant, and 10 (13%) as PCP dominant. Of the 65 patients classified as either Hipp or PCP, 19 showed Z-score greater than 1 in both the hippocampus and PCP. Of the 23 early-onset AD patients, 6, 10, and 7 were classified as no-Hipp-PCP, Hipp, and PCP, respectively. Furthermore, of the 58 late-onset AD patients, 10, 45, and 3 were classified as no-Hipp-PCP, Hipp, and PCP, respectively. When the relationship of Z-scores between the hippocampus and posterior cingulate/precuneus were analyzed for each group, the Hipp group showed a weak but significant correlation between the 2 regions (R = 0.36; p = 0.007), whereas the other groups did not (no-Hipp-PCP group: R = −0.04, p = 0.88; PCP group R = 0.12, p = 0.74).

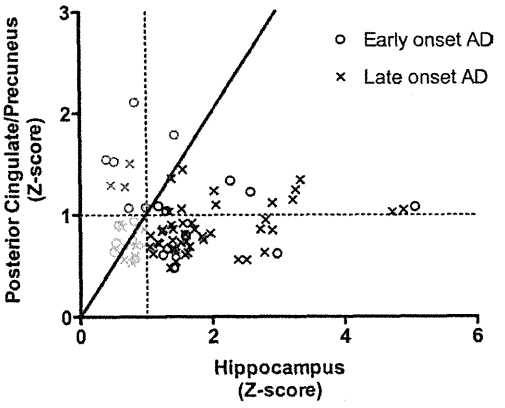

Fig. 1. Scatter plot showing the relationship of gray matter concentration loss in Alzheimer's disease (expressed as Z-score) between the hippocampus and posterior cingulate/precuneus. Green color represents no-Hipp-PCP group (no significant atrophy [Z-score of < 1.0] in hippocampus or posterior cingulate/precuneus); Black, Hipp group (hippocampal atrophy dominant); Red, PCP group (posterior cingulate/precuneus atrophy dominant). Dot lines indicate the Z-score value of 1; solid line, the line of identity.

Fig. 2 compares the degree of regional atrophy as assessed by VBM Z-scores among the groups along with normal limits (mean ± 2 SD) that was derived from 30 normal subjects. By definition, the Hipp group showed a greater degree of atrophy in the hippocampus as compared with the PCP or no-Hipp-PCP group. Additionally, this group was associated with a greater atrophy in the temporal lobe. The PCP group, on the other hand, showed a greater atrophy in the posterior cingulate/precuneus and parietal lobe. These observations persisted in all the regions after adjustment for age. The mean Z-score values in the no-Hipp-PCP group fell within the normal limits in all the

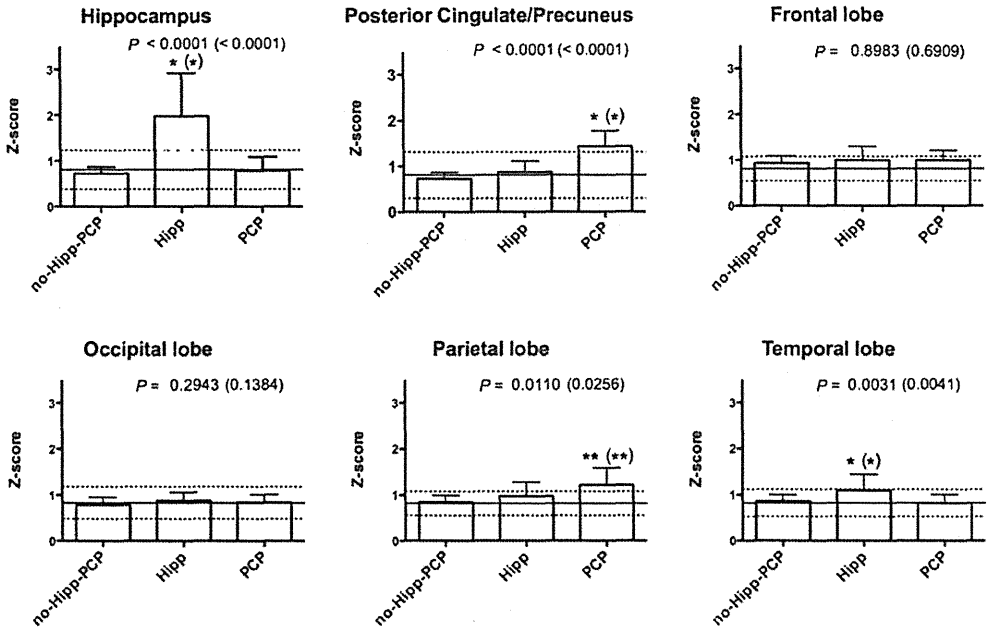

Fig. 2. Bar charts comparing the degree of atrophy (expressed as Z-score) assessed by voxel-based morphometry (VBM) in the regions of interest among Alzheimer's disease groups based on atrophic patterns. The solid and dot lines indicate the mean normal value and 2 SDs, respectively. no-Hipp-PCP indicates no significant atrophy (Z-score of < 1.0) in hippocampus or posterior cingulate/precuneus. The p value shown is based on Kruskal-Wallis test, and that in parenthesis on analysis of covariance with age adjustment. Hipp, hippocampal atrophy dominant; PCP, posterior cingulate/precuneus atrophy dominant. * and ** denote $p < 0.05$ versus the other groups, and no-Hipp-PCP, respectively.

regions. The mean differences in Z-score between hippocampus and posterior cingulate/precuneus (Z-score in the hippocampus−Z-score in the posterior cingulate/precuneus) were −0.02 ± 0.20 in the no-Hipp-PCP, 1.11 ± 0.89 in the Hipp, and −0.64 ± 0.43 in the PCP group.

Clinical characteristics and results of cognitive tests of each AD group are summarized in Tables 1 and 2. Age and age of disease onset were younger in the patients with PCP involvement. The results of APOE phenotyping, which was available in 67 patients, showed no significant differences in prevalence of ε4 carriers among the groups. Cognitive function as assessed by MMSE score was similar among the groups (mean, 22.3–22.8). The results of WAIS-R (n = 78) or WMS-R (n = 74) were available in the majority of patients. Full-scale and verbal IQ of the no-Hipp-PCP group were slightly but significantly higher than those of the Hipp group. Cognitive profile by WMS-R showed a significant decline in delayed recall along with relatively spared attention index in all groups. No-Hipp-PCP of WMS-R domains did not show a significant difference among the groups, although the verbal memory tended to be lower in the PCP group (p = 0.09).

The results of CSF biomarkers are summarized in Table 3. The PCP group had a higher p-tau level than the Hipp

Table 1
Clinical characteristics of Alzheimer's disease subgroups according to atrophic pattern

	No-Hipp-PCP (n = 16)	Hipp (n = 55)	PCP (n = 10)	p-value
Age (range)	68 ± 9 (54–79)	71 ± 7 (49–79)	60 ± 8* (47–74)	0.0002
Onset age (range)	66 ± 8 (54–77)	69 ± 6 (48–78)	58 ± 9* (45–73)	0.0002
Gender, M:F	9:7	23:32	8:2	0.07
CDR, 0.5:1	0:16	9:46	0:10	0.145*
Term of education, y	11.1 ± 2.3	10.9 ± 2.6	12.6 ± 2.0	0.135 (0.940)
APOE ε4 carrier, n	8/14 (57%)	28/46 (61%)	4/7 (57%)	1.000[a]
PET-based classification, no-Hipp-PCP:Hipp:PCP	6:0:10	9:12:34	1:0:9	0.043[a]

Data are presented as mean ± SD. No-Hipp-PCP indicates no significant atrophy (Z-score of < 1.0) in hippocampus or posterior cingulate/precuneus. p values in parentheses denote those by analysis of covariance with age adjustment.
Key: APOE, apolipoprotein E; CDR, Clinical Dementia Rating; F, female; Hipp, hippocampal atrophy dominant; M, male; PCP, posterior cingulate/precuneus atrophy dominant; PET, positron emission tomography.
[a] Tested by Fisher's exact test.
* $p < 0.05$ versus the other groups.

Table 2
Results of neuropsychological tests

	No-Hipp-PCP	Hipp	PCP	*p*-value
MMSE	$n = 16$	$n = 55$	$n = 10$	
Score	22.8 ± 2.8	22.8 ± 3.4	22.3 ± 2.6	0.899 (0.585)
WAIS-R	$n = 16$	$n = 53$	$n = 9$	
Full IQ	96.8 ± 14.2*	87.1 ± 12.3	86.9 ± 13.0	0.031 (0.032)
Verbal IQ	97.6 ± 11.7*	87.3 ± 13.3	90.4 ± 11.7	0.025 (0.036)
Performance IQ	96.0 ± 18.4	87.6 ± 14.7	84.4 ± 14.2	0.112 (0.096)
WMS-R	$n = 15$	$n = 49$	$n = 10$	
Verbal	67.9 ± 9.9	66.0 ± 10.4	58.9 ± 10.9	0.090 (0.296)
Visual	73.1 ± 18.5	64.4 ± 15.3	64.9 ± 16.5	0.185 (0.202)
General	67.1 ± 12.1	63.2 ± 11.3	57.9 ± 10.6	0.146 (0.234)
Attention	93.1 ± 13.9	87.1 ± 18.6	88.0 ± 20.9	0.534 (0.556)
Delayed	55.2 ± 6.9	56.0 ± 7.5	54.4 ± 10.8	0.832 (0.700)

Data are presented as mean ± SD. *p* values in parentheses denote those by analysis of covariance with age adjustment. No-Hipp-PCP indicates no significant atrophy (*Z*-score of < 1.0) in hippocampus or posterior cingulate/precuneus.
Key: Hipp, hippocampal atrophy dominant; MMSE, Mini Mental State Examination; PCP, posterior cingulate/precuneus atrophy dominant; WAIS-R, Wechsler Adult Intelligence Scale-Revised; WMS-R, Wechsler Memory Scale-Revised.
* $p < 0.05$ versus Hipp.

group, which persisted after adjustment for age. By contrast, Aβ42 was similar among the groups.

3.2. FDG PET *in relation to diverse atrophic patterns*

When FDG PET was used to classify the patients, the majority of patients ($n = 53$) were classified as PET-PCP; the others as PET-no-Hipp-PCP ($n = 16$) or PET-Hipp ($n = 12$). This was true in all the VBM-based groups (Table 1). Fig. 3 compares the degree of regional metabolic reduction (FDG PET *Z*-scores) among the groups along with normal limits (mean ± 2 SD). The PCP group showed a greater reduction in FDG activity in the posterior cingulate/precuneus and parietal lobe. The Hipp group showed a greater reduction in FDG activity in the hippocampus. These observations persisted in all regions except for the posterior cingulate/precuneus after adjustment for age. The mean *Z*-score values in the no-Hipp-PCP group exceeded the normal limit (mean ± 2 SD) in the parietal lobe. When *Z*-scores of FDG PET were compared with those of VBM, the degree of reduction in FDG activity was significantly greater than that in gray matter concentration in the posterior cingulate/precuneus, parietal, and temporal lobe for each group (Fig. 3). By contrast, the degree of reduction in FDG activity was less (Hipp and PCP group) than or similar (no-Hipp-PCP group) to that in gray matter concentration in the hippocampus. Representative case examples of VBM and FDG PET *Z*-score maps in each group are illustrated in Fig. 4.

Relationship between gray matter atrophy and FDG decline are summarized in Table 4. The degree of atrophy in a region (e.g., hippocampus) was significantly correlated with that of FDG decline in that region. However, the correlation coefficients between VBM and PET were variable (0.32–0.71) from region to region. Furthermore, the degree of hippocampal atrophy was significantly correlated with that of FDG decline in the temporal lobe. The degree of posterior cingulate/precuneus atrophy was correlated with that of FDG decline in the frontal, occipital, parietal, and temporal lobes.

3.3. *Effect of age on voxel-based morphometry and* FDG PET *Z-scores*

Relationship between age and VBM or FDG PET *Z*-scores are summarized in Table 5. The degree of gray matter atrophy as assessed by VBM *Z*-score was weakly and positively correlated with age in the hippocampus, and was negatively correlated with age in the posterior cingulate/precuneus. When the analysis was performed in each atrophy-based group, the no-Hipp-PCP group showed a positive correlation between the degree of atrophy and age in the frontal

Table 3
Results of CSF biomarkers

	No-Hipp-PCP ($n = 11$)	Hipp ($n = 33$)	PCP ($n = 8$)	*p* value
Phospho-tau181 (pg/mL)	74 ± 26	80 ± 59	129 ± 37*	0.006 (0.020)
Aβ42 (pg/mL)	460 ± 277	380 ± 122	384 ± 99	0.671[a] (0.409)

Data are presented as mean ± SD. *p* values in parentheses denote those by analysis of covariance with age adjustment. No-Hipp-PCP indicates no significant atrophy (*Z*-score of < 1.0) in hippocampus or posterior cingulate/precuneus.
Key: Hipp, hippocampal atrophy dominant; PCP, posterior cingulate/precuneus atrophy dominant.
[a] Tested by Welch's analysis of variance.
* $p < 0.05$ versus Hipp.

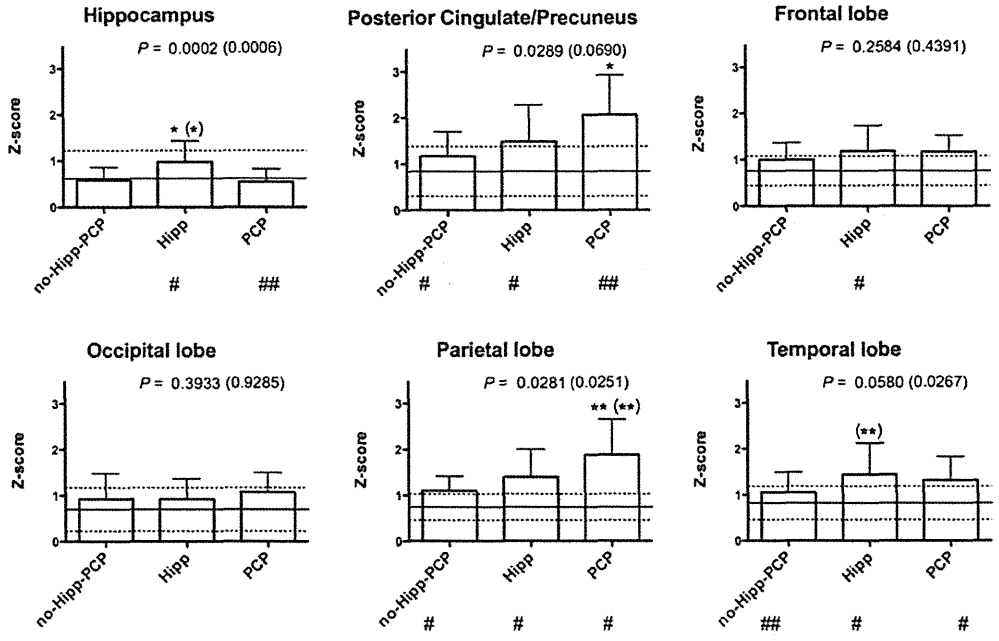

Fig. 3. Bar charts comparing the degree of ^{18}F-fluorodeoxyglucose (FDG) decline (expressed as Z-score) in the posterior cingulate gyri/parietotemporal area among Alzheimer's disease subgroups based on atrophic patterns. The solid and dot lines indicate the mean normal value and 2 SD, respectively. no-Hipp-PCP indicates no significant atrophy (Z-score of < 1.0) in hippocampus or posterior cingulate/precuneus. Hipp, hippocampal atrophy dominant; PCP, posterior cingulate/precuneus atrophy dominant. The p-value shown is based on Kruskal-Wallis test, and that in parenthesis on analysis of covariance with age adjustment. * and ** denote $p < 0.05$ versus the other groups, and no-Hipp-PCP, respectively. # and ## denote $p < 0.01$ and $p < 0.05$, respectively, versus the degree of atrophy on voxel-based morphometry (VBM) (Fig. 2) by Wilcoxon sign rank test.

lobe. The other 2 groups did not show significant correlations in any regions. On the other hand, the degree of FDG decline was weakly and negatively correlated with age in the posterior cingulate/precuneus, occipital, and parietal lobes. Although this trend was present in the no-Hipp-PCP and Hipp group, the PCP group did not show significant correlations due to the low sample size (n = 10).

4. Discussion

This study describes for the first time the relationship between diverse atrophic patterns and metabolic activity measured by FDG PET. The major findings of this study were that (1) the majority of AD patients (68%) showed a greater atrophy in the hippocampus than in the posterior cingulate/precuneus; (2) a subset of patients (denoted as the PCP group), however, revealed a greater atrophy in the posterior cingulate/precuneus than in the hippocampus, and were associated with a greater degree of metabolic reduction in the posterior cingulate/precuneus and parietal lobe; (3) the PCP group was also associated with a higher p-tau level than the Hipp group; and (4) some other patients showed no significant atrophy in either hippocampus or posterior cingulate/precuneus despite the clinical stage comparable with the other groups.

4.1. Methodological consideration

A strength of this study is the use of normal data sets strictly matched for age to individual AD patients. Although this approach requires a large number of control subjects to construct many database sets, potential age-related effects on Z-score maps due to the difference in age between each individual patient and normal database can be avoided. Another strength is related to the nature of single-center study design despite the relatively large sample size, where all patients or subjects were imaged with a single PET or MRI system using a homogeneous study protocol.

From a technical viewpoint, PVE due to the limited spatial resolution of current PET systems causes an underestimation of measured FDG activity. This is particularly an issue in measuring tracer activity in small structures such as those encountered in atrophied brain, which is common in AD patients. In this study, we used a previously established PVE correction technique that considers the diluting effects of CSF and partial volume averaging between gray and white matter, which had been validated in brain phantom, normal subjects (Yanase et al., 2005), and AD patients (Samuraki et al., 2007).

4.2. Brain structural changes in Alzheimer's disease

It is well documented that early AD-associated pathological changes first occur in the hippocampal areas, which

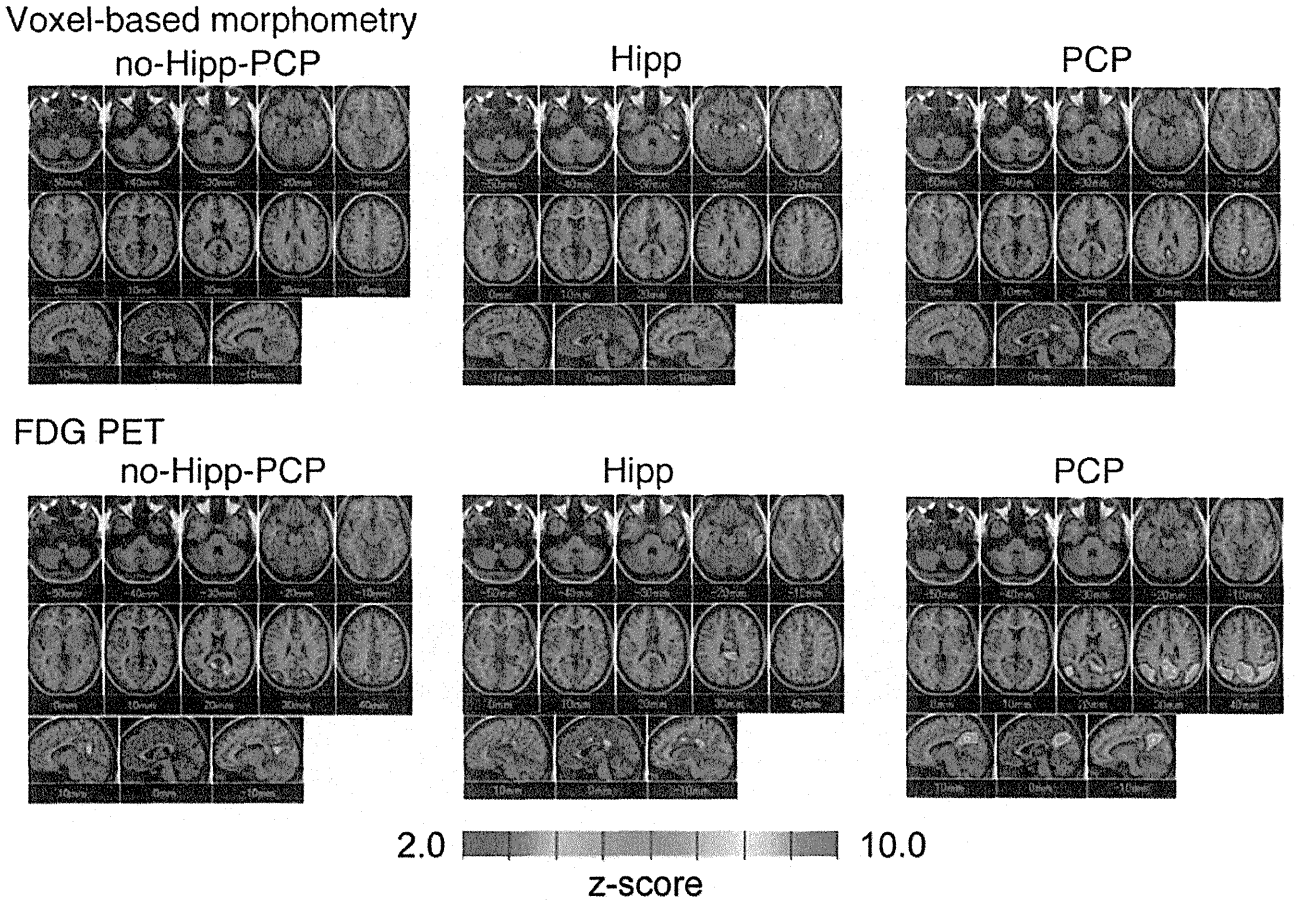

Fig. 4. Examples of voxel-based morphometry (VBM) and 18F-fluorodeoxyglucose positron emission tomography (FDG PET) Z-score maps in each Alzheimer's disease (AD) group based on atrophic pattern. Automated voxel-by-voxel Z-score analysis was performed by comparison of relative gray matter concentration or ^{18}F-FDG uptake for patient with mean and SD of gray matter or ^{18}F-FDG images of healthy volunteers. Color-scaled Z-score maps ranging from 2.0 to 10.0 were displayed by overlaying on transaxial sections of anatomically standardized magnetic resonance image (MRI) of patient. By definition, positive Z scores indicate more severe atrophy in VBM or hypometabolism in PET.

subsequently extends to the rest of brain, relatively sparing sensorimotor cortex (Braak et al., 1996). Consistent with these pathological observations, a number of structural MRI studies have demonstrated gray matter loss in the medial temporal lobe structures, including hippocampal area (Ishii et al., 2005b; Petrella et al., 2003; Whitwell et al., 2008a, 2008b). Thus, structural MRI can serve as a surrogate marker of neurodegenerative alteration in AD (Whitwell

Table 4
Correlation coefficients of Z-scores: matrix between VBM and FDG PET

	VBM					
	Hippocampus	Posterior cingulate/precuneus	Frontal lobe	Occipital lobe	Parietal lobe	Temporal lobe
PET						
Hippocampus	0.47*	0.09	0.12	0.30*	0.09	0.33*
Posterior cingulate/precuneus	0.16	0.49*	0.26**	0.26**	0.57*	0.23**
Frontal lobe	0.12	0.27**	0.61*	0.13	0.43*	0.34*
Occipital lobe	0.06	0.31*	0.15	0.32*	0.28**	0.25*
Parietal lobe	0.17	0.52*	0.25**	0.24**	0.57*	0.33*
Temporal lobe	0.41*	0.30*	0.41*	0.24**	0.46*	0.71*

Key: FDG, ^{18}F-fluorodeoxyglucose; PET, positron emission tomography; VBM, voxel-based morphometry.
* $p < 0.01$.
** $p < 0.05$.

Table 5
Correlation coefficients: matrix between Age and VBM or FDG PET Z-scores

	Hippocampus	Posterior cingulate/precuneus	Frontal lobe	Occipital lobe	Parietal lobe	Temporal lobe
VBM						
All (n = 81)	0.24**	−0.33*	0.11	−0.08	−0.21	0.06
No-Hipp-PCP (n = 16)	0.30	−0.19	0.58**	−0.50	0.03	−0.09
Hipp (n = 55)	0.06	−0.05	0.06	0.04	−0.12	−0.06
PCP (n = 10)	−0.02	−0.34	−0.07	−0.37	−0.28	−0.40
PET						
All (n = 81)	0.11	−0.34*	0.001	−0.28**	−0.36*	−0.17
No-Hipp-PCP (n = 16)	−0.17	−0.56**	0.25	−0.33	−0.09	−0.39
Hipp (n = 55)	0.09	−0.31**	−0.03	−0.34**	−0.33**	−0.20
PCP (n = 10)	−0.34	−0.48	−0.39	0.26	−0.51	−0.48

No-Hipp-PCP indicates no significant atrophy (Z-score of < 1.0) in hippocampus or posterior cingulate/precuneus.
Key: FDG, ^{18}F-fluorodeoxyglucose; Hipp, hippocampal atrophy dominant; PCP, posterior cingulate/precuneus atrophy dominant; PET, positron emission tomography; VBM, voxel-based morphometry.
* $p < 0.01$.
** $p < 0.05$.

et al., 2008a). Keeping these in mind, our observation that the hippocampal atrophy was dominant (the Hipp group) in the majority of patients generally agrees with the concept described above. It is notable, however, our results demonstrated that the posterior cingulate/precuneus dominant atrophy occurs in a subset of patients (the PCP group), where Braak AD staging (Braak et al., 1996; Whitwell et al., 2007) may not fit very well. So far, diverse results have been reported regarding the presence or absence of posterior cingulate/precuneus atrophy in AD (Chételat et al., 2008; Frisoni et al., 2007; Shiino et al., 2006; Whitwell et al., 2007). Furthermore, age-related atrophy is reported to occur in this region (Shiino et al., 2006). This may explain why prior studies often failed to show posterior cingulate/precuneus atrophy particularly using group comparisons between AD and control subjects. By looking at Z-score maps of individual AD patients using strictly age-matched normal databases, our data clearly indicate that posterior cingulate/precuneus atrophy truly occurs in some AD patients, and is not the result of normal aging. Although the precise mechanisms for the posterior cingulate/precuneus atrophy are not clear, it could be caused by remote effects from interconnected areas such as the medial temporal lobe, direct effects as indicated by intense amyloid deposition (Jack et al., 2008), or both. Surprisingly, a considerable number (approximately 20%) of AD patients showed no significant atrophy in either hippocampus or posterior cingulate/precuneus despite the cognitive function comparable with the other groups as assessed by MMSE score. This indicates that not only the pattern but the degree of atrophy are variable in a spectrum of AD. This group may represent the earliest manifestation of clinical AD with minimal pathological burden as assessed by structural MRI, although none of clinical features such as age, CDR, educational level, and APOE typing were specific for this group. Thus, our data indicate that there are diverse atrophic patterns in a spectrum of AD, and that clinical features cannot necessarily distinguish such atrophic patterns.

4.3. Metabolic alteration in relation to atrophy

Metabolic reduction in the posterior cingulate/precuneus and parietal lobe is a known feature of AD even at the early stage (Chételat et al., 2008; Jack et al., 2010; Minoshima et al., 1997). Our results on FDG PET-based classification is consistent with this concept in that the majority of patients showed a greater metabolic decline in the posterior cingulate/precuneus than in the hippocampus in all VBM-based groups. In this study, the PCP group had a greater metabolic reduction in the posterior cingulate/precuneus and parietal lobe than the other groups, indicating a greater metabolic burden. It should be noted that the greater metabolic reduction in this group was present even with PVE correction, indicating the observed metabolic reduction was not the result of atrophy. In this respect, the the PCP group may be regarded as an aggressive form of AD as compared with the Hipp or no-Hipp-PCP group. Our results also showed that the degree of metabolic alteration is generally greater than that of atrophy in the posterior cingulate/precuneus, parietal, and temporal lobes, which is in agreement with the literature (Chételat et al., 2008). It is noteworthy that the greater metabolic reduction than atrophy was present even in the no-Hipp-PCP group, where structural MRI showed minimal AD-related changes. This AD group may not be identified by structural imaging alone, and thus metabolic alteration in the posterior cingulate/precuneus and/or parietal lobe is a more sensitive marker of AD than structural changes. In contrast to the greater FDG decline observed in the neocortical area, the degree of FDG decline in the hippocampus was less than or similar to that of atrophy, indicating the relatively preserved metabolic activity in this region. This is in line with recent studies by our group (Samuraki et al., 2007) and by Chetelat et al. (2008) suggesting the presence of synaptic compensatory mechanisms to maintain neuronal activity despite the structural changes.

Our data showed that, although the degree of atrophy in a region was significantly correlated with that of FDG

decline in that region, the correlation coefficients were variable from region to region. This indicates that the relationship between brain structure and glucose metabolism is not simple, and that the degree of FDG decline may not be inferred from structural imaging alone. Furthermore, the degree of regional atrophy was associated with that of FDG decline in other regions, suggesting the presence of a remote effect of regional atrophy on glucose metabolism.

4.4. CSF *biomarkers and cognitive profile in relation to atrophy*

AD is known to be associated with decreased Aβ42 and increased p-tau level in CSF (Marksteiner et al., 2007). CSF Aβ42 is regarded as the earliest marker of AD in accordance with abnormal processing of amyloid precursor protein that precedes clinical symptoms (Jack et al., 2010). By contrast, p-tau reflects NFTs and hence, is thought to be a more direct marker of neuronal damage (Jack et al., 2010), which may be associated with a more rapid cognitive decline (Snider et al., 2009). In this respect, the higher p-tau level observed in the PCP group may further support the disease aggressiveness in view of CSF biomarkers, in addition to the greater metabolic burden in this group as mentioned earlier.

From a clinical viewpoint, a careful neuropsychological assessment is mandatory to carefully describe the different AD subtypes because this is to define the different neuropsychological profiles among groups. Therefore, we performed more detailed neuropsychological tests (WMS-R and WAIS-R) than MMSE in the current study. As expected, all AD groups showed a significant decline in delayed recall along with relatively spared attention index, which is consistent with early stage AD. In a study by Koric et al. (2010), atypical early-onset AD, in which symptoms other than episodic memory loss such as language, visual, and behavioral deficits reflecting neocortical involvement predominate, were associated with higher levels of p- or total tau in CSF as compared with typical (memory loss) early-onset AD, whereas levels of Aβ42 were similar between the 2 groups. The relationship of CSF biomarkers between the atypical and typical early-onset AD in their study is similar to that observed between the PCP and Hipp group in the current study. Although our results did not reach statistically significant differences in cognitive profile (e.g., visual memory and attention index) among the groups as assessed by WMS-R, there was a trend toward lower verbal memory in the PCP group, which is in line with that reported for atypical early-onset AD (Koric et al., 2010).

In this study, the no-Hipp-PCP group performed slightly better on WAIS-R (full IQ and verbal IQ) than did the Hipp group, reflecting the minimal neuronal damage as assessed by VBM and FDG PET. However, the cognitive profile of this group as assessed by WMS-R was comparable to that of the other AD groups with a significant decline in delayed recall along with relatively spared attention index. The MMSE score was also comparable to the other groups. Thus, this group seems to be difficult to characterize clinically based on these cognitive data.

4.5. *Relation to early- and late-onset Alzheimer's disease*

Although AD is considered to be a single disease entity based on the neuropathological hallmarks, many studies have shown 2 different phenotypes of AD (i.e., early- and late-onset AD) (Frisoni et al., 2005, 2007; Ishii et al., 2005a; Jack et al., 2010; Matsunari et al., 2007; Rabinovici et al., 2010). As compared with late-onset AD, the early-onset AD is reportedly associated with more neocortical atrophy, including posterior cingulate and temporoparietal junction (Frisoni et al., 2005, 2007; Ishii et al., 2005a; Shiino et al., 2006), and with lower glucose metabolism in the in posterior cingulate/precuneus, lateral temporoparietal and occipital cortices (Ishii et al., 2006; Rabinovici et al., 2010). These observations indicate that early-onset AD shares structural and metabolic features similar to those observed in the PCP group, which is supported by the younger age of this group in the current study. The onset age of the no-Hipp-PCP group, on the other hand, was at the boundary between early- and late-onset AD or between the PCP and Hipp group. Therefore, the no-Hipp-PCP group may be considered to be a "mixed" group, where the patients in this group may develop posterior cingulate/precuneus and/or hippocampal atrophy at a later stage.

In order to further characterize the aging effects on imaging results, we analyzed the relationship between age and VBM or FDG PET Z-scores as presented in Table 5. Our data showed that the aging effect is present on the degree of regional atrophy and metabolic decline despite the use of age-specific normal databases. The results indicate that the younger patients are likely to be associated with more posterior cingulate/precuneus atrophy and FDG decline, and less hippocampal atrophy, which is consistent with early-onset AD as described above. Although this trend seemed to be partially present even when each group was separately analyzed, it was difficult to characterize individual groups because of the limited number of patients in each group.

4.6. *Limitations of the study*

There are limitations of the study that should be mentioned. First, the diagnosis of probable AD was made based on clinical examinations, and therefore may differ from that obtained from final pathologic verification; a limitation present in many of such studies. However, it has been reported that the diagnostic accuracy can exceed 90% in an academic memory disorders clinical setting (Rasmusson et al., 1996), which was the case in this study. Second, this is a cross-sectional study and longitudinal data were not obtained. Therefore, whether the disease progression would cause a conversion of atrophic patterns (e.g., from the PCP to the Hipp group) at a later stage remains unknown. How-

ever, the primary goal of this study was to metabolically and biologically characterize AD patients at mild clinical stage based on atrophic patterns, which was well achieved in the current study. Third, we measured p-tau and Aβ but not total tau in this study. This was because total tau can be viewed as a nonspecific marker of neuronal damage (Blennow and Hampel, 2003). However, it is possible that total tau measurement may have provided a more comprehensive understanding of underlying pathophysiology. Fourth, amyloid imaging such as ^{11}C-Pib PET (Jack et al., 2008) was not performed in this study. Therefore, possible differences in regional amyloid burden among the atrophy-based groups could not be addressed. Nevertheless, global amyloid burden as assessed by CSF Aβ42 does not seem to be different among the groups. Finally, CSF analysis was made based on a small number of patients (PCP = 8), which may have impaired the clear-cut interpretation of data. Therefore, the results as to the relationship between AD subgroup and p-tau should be regarded as preliminary until confirmed in further studies, although the p-tau level was significantly higher in the PCP group.

4.7. Conclusions

There are diverse atrophic patterns that exist in a spectrum of AD despite the comparable clinical stage, which are associated with different degrees of metabolic abnormalities and p-tau levels. In particular, a subset of AD patients show greater atrophy in the posterior cingulate/precuneus rather than in the hippocampus, where Braak AD staging may not fit very well. These patients are relatively young, and are considered to be an extensive form of AD as reflected by a more severe degree of metabolic reduction and higher CSF p-tau level. Thus, AD may be a more complex disease entity than previously thought from structural, metabolic, and biological perspectives.

Disclosure statement

None of the authors have conflicts to disclose.

The study protocol was approved by the institutional ethical committee and written informed consent was obtained from all subjects before participation in the study.

Acknowledgements

This study was supported in part by a grant for Development of Advanced Technology for Measurement and Evaluation of Brain Functions, Ishikawa Prefecture Collaboration of Regional Entities for the Advancement of Technological Excellence (to MY), from Japan Science and Technology Corporation, Japan, and by a grant for the Knowledge Cluster Initiative (High-Tech Sensing and Knowledge Handling Technology [Brain Technology]) (to MY) from the Japanese Ministry of Education, Culture, Sports, Science and Technology, Japan, and by Ishikawa Prefectural Government (to IM).

References

Blennow, K., Hampel, H., 2003. CSF markers for incipient Alzheimer's disease. Lancet Neurol. 2, 605–613.

Braak, H., Braak, E., Yilmazer, D., de Vos, R.A., Jansen, E.N., Bohl, J., 1996. Pattern of brain destruction in Parkinson's and Alzheimer's diseases. J. Neural Transm. 103, 455–490.

Chen, W.P., Samuraki, M., Yanase, D., Shima, K., Takeda, N., Ono, K., Yoshita, M., Nishimura, S., Yamada, M., Matsunari, I., 2008. Effect of sample size for normal database on diagnostic performance of brain FDG PET for the detection of Alzheimer's disease using automated image analysis. Nucl. Med. Commun. 29, 270–276.

Chételat, G., Desgranges, B., Landeau, B., Mézenge, F., Poline, J.B., de la Sayette, V., Viader, F., Eustache, F., Baron, J.C., 2008. Direct voxel-based comparison between grey matter hypometabolism and atrophy in Alzheimer's disease. Brain 131, 60–71.

Frisoni, G.B., Pievani, M., Testa, C., Sabattoli, F., Bresciani, L., Bonetti, M., Beltramello, A., Hayashi, K.M., Toga, A.W., Thompson, P.M., 2007. The topography of grey matter involvement in early and late onset Alzheimer's disease. Brain 130, 720–730.

Frisoni, G.B., Testa, C., Sabattoli, F., Beltramello, A., Soininen, H., Laakso, M.P., 2005. Structural correlates of early and late onset Alzheimer's disease: voxel based morphometric study. J. Neurol. Neurosurg., Psychiatry 76, 112–114.

Good, C.D., Johnsrude, I.S., Ashburner, J., Henson, R.N., Friston, K.J., Frackowiak, R.S., 2001. A voxel-based morphometric study of ageing in 465 normal adult human brains. Neuroimage 14, 21–36.

Herholz, K., Salmon, E., Perani, D., Baron, J.C., Holthoff, V., Frölich, L., Schönknecht, P., Ito, K., Mielke, R., Kalbe, E., Zündorf, G., Delbeuck, X., Pelati, O., Anchisi, D., Fazio, F., Kerrouche, N., Desgranges, B., Eustache, F., Beuthien-Baumann, B., Menzel, C., Schröder, J., Kato, T., Arahata, Y., Henze, M., Heiss, W.D., 2002. Discrimination between Alzheimer dementia and controls by automated analysis of multicenter FDG PET. Neuroimage 17, 302–316.

Hughes, C.P., Berg, L., Danziger, W.L., Coben, L.A., Martin, R.L., 1982. A new clinical scale for the staging of dementia. Br. J. Psychiatry 140, 566–572.

Ishii, K., Kawachi, T., Sasaki, H., Kono, A.K., Fukuda, T., Kojima, Y., Mori, E., 2005a. Voxel-based morphometric comparison between early- and late-onset mild Alzheimer's disease and assessment of diagnostic performance of z score images. AJNR Am. J. Neuroradiol. 26, 333–340.

Ishii, K., Kono, A.K., Sasaki, H., Miyamoto, N., Fukuda, T., Sakamoto, S., Mori, E., 2006. Fully automatic diagnostic system for early- and late-onset mild Alzheimer's disease using FDG PET and 3D-SSP. Eur. J. Nucl. Med. Mol. Imaging 33, 575–583.

Ishii, K., Sasaki, H., Kono, A.K., Miyamoto, N., Fukuda, T., Mori, E., 2005b. Comparison of gray matter and metabolic reduction in mild Alzheimer's disease using FDG-PET and voxel-based morphometric MR studies. Eur. J. Nucl. Med. Mol. Imaging 32, 959–963.

Jack, C.R., Jr., Knopman, D.S., Jagust, W.J., Shaw, L.M., Aisen, P.S., Weiner, M.W., Petersen, R.C., Trojanowski, J.Q., 2010. Hypothetical model of dynamic biomarkers of the Alzheimer's pathological cascade. Lancet Neurol. 9, 119–128.

Jack, C.R., Jr., Lowe, V.J., Senjem, M.L., Weigand, S.D., Kemp, B.J., Shiung, M.M., Knopman, D.S., Boeve, B.F., Klunk, W.E., Mathis, C.A., Petersen, R.C., 2008. 11C PiB and structural MRI provide complementary information in imaging of Alzheimer's disease and amnestic mild cognitive impairment. Brain 131, 665–680.

Kataoka, S., Paidi, M., Howard, B.V., 1994. Simplified isoelectric focusing/immunoblotting determination of apoprotein E phenotype. Clin. Chem. 40, 11–13.

Koric, L., Felician, O., Guedj, E., Hubert, A.M., Mancini, J., Boucraut, J., Ceccaldi, M., 2010. Could clinical profile influence CSF biomarkers in early-onset Alzheimer disease? Alzheimer Dis. Assoc. Disord. 24, 278–283.

Maldjian, J.A., Laurienti, P.J., Kraft, R.A., Burdette, J.H., 2003. An automated method for neuroanatomic and cytoarchitectonic atlas-based interrogation of fMRI data sets. Neuroimage 19, 1233–1239.

Marksteiner, J., Hinterhuber, H., Humpel, C., 2007. Cerebrospinal fluid biomarkers for diagnosis of Alzheimer's disease: beta-amyloid(1–42), tau, phospho-tau-181 and total protein. Drugs Today (Barc.) 43, 423–431.

Matsuda, H., 2007. Role of neuroimaging in Alzheimer's Disease, with emphasis on brain perfusion SPECT. J. Nucl. Med. 48, 1289–1300.

Matsuda, H., Ohnishi, T., Asada, T., Li, Z.J., Kanetaka, H., Imabayashi, E., Tanaka, F., Nakano, S., 2003. Correction for partial-volume effects on brain perfusion SPECT in healthy men. J. Nucl. Med. 44, 1243–1252.

Matsumoto, Y., Yanase, D., Noguchi-Shinohara, M., Ono, K., Yoshita, M., Yamada, M., 2007. Blood-brain barrier permeability correlates with medial temporal lobe atrophy but not with amyloid-beta protein transport across the blood-brain barrier in Alzheimer's disease. Dement. Geriatr. Cogn. Disord. 23, 241–245.

Matsunari, I., Samuraki, M., Chen, W.P., Yanase, D., Takeda, N., Ono, K., Yoshita, M., Matsuda, H., Yamada, M., Kinuya, S., 2007. Comparison of ^{18}F-FDG PET and Optimized Voxel-Based Morphometry for Detection of Alzheimer's Disease: Aging Effect on Diagnostic Performance. J. Nucl. Med. 48, 1961–1970.

McKhann, G., Drachman, D., Folstein, M., Katzman, R., Price, D., Stadlan, E.M., 1984. Clinical diagnosis of Alzheimer's disease: report of the NINCDS-ADRDA Work Group under the auspices of Department of Health and Human Services Task Force on Alzheimer's Disease. Neurology 34, 939–944.

Minoshima, S., Giordani, B., Berent, S., Frey, K.A., Foster, N.L., Kuhl, D.E., 1997. Metabolic reduction in the posterior cingulate cortex in very early Alzheimer's disease. Ann. Neurol. 42, 85–94.

Morinaga, A., Ono, K., Ikeda, T., Ikeda, Y., Shima, K., Noguchi-Shinohara, M., Samuraki, M., Yanase, D., Yoshita, M., Iwasa, K., Mastunari, I., Yamada, M., 2010. A Comparison of the diagnostic sensitivity of MRI, CBF-SPECT, FDG-PET and cerebrospinal fluid biomarkers for detecting Alzheimer's disease in a memory clinic. Dement. Geriatr. Cogn. Disord. 30, 285–292.

Petrella, J.R., Coleman, R.E., Doraiswamy, P.M., 2003. Neuroimaging and early diagnosis of Alzheimer disease: a look to the future. Radiology 226, 315–336.

Rabinovici, G.D., Furst, A.J., Alkalay, A., Racine, C.A., O'Neil, J.P., Janabi, M., Baker, S.L., Agarwal, N., Bonasera, S.J., Mormino, E.C., Weiner, M.W., Gorno-Tempini, M.L., Rosen, H.J., Miller, B.L., Jagust, W.J., 2010. Increased metabolic vulnerability in early-onset Alzheimer's disease is not related to amyloid burden. Brain 133, 512–528.

Rasmusson, D.X., Brandt, J., Steele, C., Hedreen, J.C., Troncoso, J.C., Folstein, M.F., 1996. Accuracy of clinical diagnosis of Alzheimer disease and clinical features of patients with non-Alzheimer disease neuropathology. Alzheimer Dis. Assoc. Disord. 10, 180–188.

Samuraki, M., Matsunari, I., Chen, W.P., Yajima, K., Yanase, D., Fujikawa, A., Takeda, N., Nishimura, S., Matsuda, H., Yamada, M., 2007. Partial volume effect-corrected FDG PET and grey matter volume loss in patients with mild Alzheimer's disease. Eur. J. Nucl. Med. Mol. Imaging 34, 1658–1669.

Shiino, A., Watanabe, T., Maeda, K., Kotani, E., Akiguchi, I., Matsuda, M., 2006. Four subgroups of Alzheimer's disease based on patterns of atrophy using VBM and a unique pattern for early onset disease. Neuroimage 33, 17–26.

Snider, B.J., Fagan, A.M., Roe, C., Shah, A.R., Grant, E.A., Xiong, C., Morris, J.C., Holtzman, D.M., 2009. Cerebrospinal fluid biomarkers and rate of cognitive decline in very mild dementia of the Alzheimer type. Arch. Neurol. 66, 638–645.

Tang-Wai, D.F., Graff-Radford, N.R., Boeve, B.F., Dickson, D.W., Parisi, J.E., Crook, R., Caselli, R.J., Knopman, D.S., Petersen, R.C., 2004. Clinical, genetic, and neuropathologic characteristics of posterior cortical atrophy. Neurology 63, 1168–1174.

Tapiola, T., Overmyer, M., Lehtovirta, M., Helisalmi, S., Ramberg, J., Alafuzoff, I., Riekkinen, P., Sr., Soininen, H., 1997. The level of cerebrospinal fluid tau correlates with neurofibrillary tangles in Alzheimer's disease. Neuroreport 8, 3961–3963.

Tzourio-Mazoyer, N., Landeau, B., Papathanassiou, D., Crivello, F., Etard, O., Delcroix, N., Mazoyer, B., Joliot, M., 2002. Automated anatomical labeling of activations in SPM using a macroscopic anatomical parcellation of the MNI MRI single-subject brain. Neuroimage 15, 273–289.

van der Vlies, A.E., Verwey, N.A., Bouwman, F.H., Blankenstein, M.A., Klein, M., Scheltens, P., van der Flier, W.M., 2009. CSF biomarkers in relationship to cognitive profiles in Alzheimer disease. Neurology 72, 1056–1061.

Wechsler, D., 1981. Wechsler Adult Intelligence Scale: Revised. Psychological Corporation, New York.

Wechsler, D., 1987. Wechsler Memory Scale: Revised. The Psychological Corporation, San Antonio.

Whitwell, J.L., Josephs, K.A., Murray, M.E., Kantarci, K., Przybelski, S.A., Weigand, S.D., Vemuri, P., Senjem, M.L., Parisi, J.E., Knopman, D.S., Boeve, B.F., Petersen, R.C., Dickson, D.W., Jack, C.R., Jr., 2008a. MRI correlates of neurofibrillary tangle pathology at autopsy: a voxel-based morphometry study. Neurology 71, 743–749.

Whitwell, J.L., Przybelski, S.A., Weigand, S.D., Knopman, D.S., Boeve, B.F., Petersen, R.C., Jack, C.R., Jr., 2007. 3D maps from multiple MRI illustrate changing atrophy patterns as subjects progress from mild cognitive impairment to Alzheimer's disease. Brain 130, 1777–1786.

Whitwell, J.L., Shiung, M.M., Przybelski, S.A., Weigand, S.D., Knopman, D.S., Boeve, B.F., Petersen, R.C., Jack, C.R., Jr., 2008b. MRI patterns of atrophy associated with progression to AD in amnestic mild cognitive impairment. Neurology 70, 512–520.

Yanase, D., Matsunari, I., Yajima, K., Chen, W., Fujikawa, A., Nishimura, S., Matsuda, H., Yamada, M., 2005. Brain FDG PET study of normal aging in Japanese: effect of atrophy correction. Eur. J. Nucl. Med. Mol. Imaging 32, 794–805.

NEUROPATHOLOGY

Neuropathology 2013; **33**, 47–58 doi:10.1111/j.1440-1789.2012.01329.x

Original Article

Neuropathologic analysis of Lewy-related α-synucleinopathy in olfactory mucosa

Sayaka Funabe,[1,4] Masaki Takao,[1] Yuko Saito,[5] Hiroyuki Hatsuta,[1] Mikiko Sugiyama,[1] Shinji Ito,[1] Kazutomi Kanemaru,[2] Motoji Sawabe,[3] Tomio Arai,[3] Hideki Mochizuki,[6] Nobutaka Hattori[4] and Shigeo Murayama[1]

Departments of [1]Neuropathology, [2]Neurology, [3]Pathology, Tokyo Metropolitan Geriatric Hospital and Institute of Gerontology, [4]Department of Neurology, Juntendo University, [5]Department of Laboratory Medicine, National Center Hospital for Neurology and Psychiatry, Tokyo and [6]Department of Neurology, Faculty of Medicine, Osaka University, Osaka, Japan

We analyzed the incidence and extent of Lewy-related α-synucleinopathy (LBAS) in the olfactory mucosa, as well as the central and peripheral nervous systems of consecutive autopsy cases from a general geriatric hospital. The brain and olfactory mucosa were immunohistochemically examined using antibodies raised against phosphorylated α-synuclein. Thirty-nine out of 105 patients (37.1%) showed LBAS in the central or peripheral nervous systems. Seven patients presented LBAS (Lewy neurites) in the olfactory lamina propria mucosa. One out of the seven cases also showed a Lewy neurite in a bundle of axons in the cribriform plate, but α-synuclein deposits were not detected in the olfactory receptor neurons. In particular, high incidence of α-synuclein immunopositive LBAS in the olfactory mucosa was present in the individuals with clinically as well as neuropathologically confirmed Parkinson's disease and dementia with Lewy bodies (6/8 cases, 75%). However, this pathologic alteration was rare in the cases with incidental or subclinical Lewy body diseases (LBD) (one out of 31 cases, 3.2%). In the olfactory bulb, the LBAS was usually present in the glomeruli and granular cells of most symptomatic and asymptomatic cases with LBD. Our studies further confirmed importance of the olfactory entry zone in propagation of LBAS in the human aging nervous system.

Key words: α-synuclein, Lewy body, neuropathology, olfactory mucosa, Parkinson's disease.

Correspondence: Shigeo Murayama, MD, PhD, Department of Neuropathology, Tokyo Metropolitan Geriatric Hospital and Institute of Gerontology, 35-2, Sakae-cho, Itabashi-ku, Tokyo 173-0015, Japan. Email: smurayam@tmig.or.jp

Received 30 March 2012; revised and accepted 19 April 2012; published online 4 June 2012.

INTRODUCTION

Sporadic Parkinson's disease is a neurodegenerative disorder characterized clinically by resting tremor, rigidity, bradykinesia and gait disturbance, as well as neuropathologically by the loss of neurons in several brainstem nuclei and the presence of Lewy bodies formed by abnormal accumulation of α-synuclein.[1–5] Of the many types of neurons in the central and peripheral nervous systems, a specific subset of neurons is vulnerable to accumulation of α-synuclein, which takes the form of aggregates such as Lewy bodies and Lewy neurites (LBs/LNs).[6–8]

Based on studies of a large number of autopsy cases, the initial sites involved in Lewy-related pathology are reported to be the dorsal motor nucleus of the vagus, the intermediate reticular zone in the lower brainstem and olfactory bulb.[9,10] We previously reported that in the earliest stage of Lewy-related α-synucleinopathy (LBAS), abnormal α-synuclein accumulation extends from the peripheral part of the olfactory bulb to the anterior olfactory nucleus as well as the amygdala.[11] From a clinical standpoint, impaired olfactory function constitutes one of the earliest symptoms of sporadic Parkinson's disease.[12,13] Therefore, the olfactory system may be one of the vital regions in the development of Lewy body disease (LBD).

In the olfactory bulb, α-synuclein accumulation is observed in the anterior olfactory nucleus as well as the mitral, tufted, and granular cells of individuals with clinical Parkinson's disease or dementia with Lewy bodies (DLB). Even in the early stages of these diseases, LNs, LBs or both, can be seen in the olfactory bulbs.[11,14,15] Based on the results of a neuropathologic study, Beach *et al.* suggested that the olfactory bulb may be a candidate region of biopsy study to

confirm the diagnosis of LBD.[16] However, the biopsy of olfactory bulb is too invasive and difficult to carry out for patients without risk.[17,18]

The olfactory epithelium is composed of paraneurons and neurites from which the glomeruli of the olfactory bulb originate. However, a neuropathologic analysis of LBAS has not been carried out adequately for LBD. Duda *et al.* reported that normal α-synuclein is expressed in the basal cells, olfactory receptor neurons, supporting cells, and Bowman's glands of the olfactory epithelium in normal controls, as well as patients with Parkinson's disease, Alzheimer disease and multiple system atrophy.[19] However, pathologic α-synuclein accumulation is rare (3.7%) among both normal controls and individuals affected by DLB, Alzheimer disease or Parkinson's disease.[20] According to a biopsy study of the olfactory epithelium in individuals with Parkinson's disease and younger hyposmic controls, no specific pathologic alteration was found.[21]

Therefore, it is still controversial whether abnormal α-synuclein accumulation in the olfactory epithelium precedes the formation of LBs/LNs in the olfactory bulb and contributes to olfactory dysfunction in sporadic Parkinson's disease. The aim of this study was to clarify the neuropathologic alterations of the olfactory mucosa in LBD by immunohistochemical analysis of a series of autopsied individuals.

MATERIALS AND METHODS

Tissue source

Tissue samples were obtained from autopsy materials that were collected at the Tokyo Metropolitan Geriatric Hospital and Institute of Gerontology between October 2008 and August 2010. This hospital is located at the center of Tokyo city and is a geriatric general emergency hospital with 579 beds. This hospital provides community-based medical service to the aged population 24 h/day in cooperation with local general practitioners. The number of autopsy cases was 162 in the above duration. In addition to the general organs, we could obtain the brains and spinal cords from 105 cases in that period, that were registered to the Brain Bank for Aging Research (BBAR) with the deceased's relatives' informed consent. The BBAR is approved by the ethics committee of the Tokyo Metropolitan Geriatric Hospital and Institute of Gerontology to carry out comprehensive research.

Clinical information

All clinical information, including the presence or absence of Parkinsonism as well as dementia, was retrospectively obtained from medical charts and reviewed by two board-certified neurologists.[11,22–26] First, we evaluated Parkinsonism such as bradykinesia, resting tremor, rigidity and postural instability. In this study, when individuals had two or more of these four clinical symptoms, we defined them as having Parkinson's disease-related symptoms.[27] Second, we analyzed scores for the Mini-Mental State Examination[28] or the Hasegawa Dementia Scale (or its revised version),[29,30] the Instrumental Activities of Daily Living,[31] and the Clinical Dementia Rating (CDR).[32] When individuals were not assigned to a category of CDR, we retrospectively determined CDR using medical records, including the battery of cognitive tests above, as well as interviews with attending physicians and caregivers when necessary. Based on these results, we assigned a clinical diagnosis to each patient. The clinical diagnosis of Alzheimer disease was carried out based on the criteria of the National Institute of Neurological and Communication Disorders and Stroke-Alzheimer Disease and Related Disorders Association.[33] The diagnosis of DLB and Parkinson's disease with dementia conformed to the third report of the DLB consortium.[34]

Histology

We examined the brain and olfactory epithelium, olfactory bulb, esophagogastric mucosal junction, sympathetic ganglia, thoracic spinal cord, adrenal glands, anterior wall of the left ventricle of the heart, and abdominal skin.[22,26] The brains and spinal cords were examined as previously reported.[22,24,25] Briefly, the cerebral and cerebellar hemispheres as well as brainstem were dissected in the sagittal plane at the time of autopsy. In each case, half of the brain was preserved at −80°C for further biochemical and molecular analyses. The other half of the brain and abdominal skin were fixed in 20% buffered formalin (WAKO, Osaka, Japan) for 7–13 days and sliced in the same manner as the contralateral hemisphere. The adrenal gland and anterior wall of the left ventricle of the heart were fixed in 20% formalin. The representative areas were embedded in paraffin. Six-micrometer-thick serial sections were cut and stained with HE and KB. Sections of the amygdala, hippocampus, parahippocampal gyrus and temporal cortex were stained with the modified Gallyas-Braak method for senile plaques, NFTs and argyrophilic grains.[35]

Immunohistochemistry

Sections were immunostained using the following antibodies raised against phosphorylated tau protein (p-tau) (AT8, monoclonal; Innogenetics, Temse, Belgium): synthetic peptide corresponding to amino acids 11–28 of amyloid-beta protein (12B2, monoclonal; IBL, Maebashi, Japan); phosphorylated α-synuclein (pSyn#64, monoclonal[25] and

Table 1 Antibodies used for immunohistochemistry

Antibody	Epitope	Source	Clone	Dilution ratio	Antigen method	Retrieval (min)
pSyn#64	α-synuclein phosphorylated ser 129	T. Iwatsubo	Monoclonal	1:20000	99% formic acid	5
PSer129	α-synuclein phosphorylated ser 129	T. Iwatsubo	Polyclonal	1:100	None	
PGP9.5	PGP9.5	Biomol	Polyclonal	1:5000	microwave	30
SMI31	phosphorylated neurofilament	Sternberger	Monoclonal	1:20000	None	
Tyrosine hydroxylase	Anti-tyrosine hydroxylase, rat	CALBIOCHEM	Monoclonal	1:10	microwave	30
AT8	Phosphorylated tau protein	Innogenetics	Monoclonal	1:1000	None	
12B2	Aβ11–28	IBL	Monoclonal	1:50	99% formic acid	5

PSer129 polyclonal[36]), ubiquitin (polyclonal, Sigma-Aldrich, St. Louis, MO), Protein Gene Product 9.5 (PGP9.5, polyclonal; ENZO Life Sciences International, Farmingdale, NY USA); phosphorylated neurofilament (SMI31, monoclonal; Sternberger Immunochemicals, Bethesda, MA, USA); and tyrosine hydroxylase (Anti-Tyrosine Hydroxylase, Rat, monoclonal; Calbiochem-Novabiochem Corporation, Darmstadt, Germany) (Table 1). The signals from monoclonal and polyclonal antibodies were detected by using the automatic system on a VENTANA NX20 with the I-View DAB Universal Kit (Roche, Basel, Switzerland) according to the manufacturer's instructions. Sections were counter-stained with hematoxylin.

LBAS

CNS

In order to analyze LBAS,[22] we carried out immunohistochemical analysis with phosphorylated α-synuclein antibodies for the following sections: the medulla oblongata at the level of the dorsal motor nucleus of the vagus, the upper pons at the level of the locus coeruleus, and the midbrain including the substantia nigra, amygdala, anterior hippocampus and the peripheral nervous system from all cases (described in the next section). When immunopositive deposits were observed in these anatomic regions, we carried out additional immunohistochemical analysis for sections of the basal nucleus of Meynert, anterior cingulate gyrus, entorhinal cortex, the second frontal and temporal gyri and the supramarginal gyrus, using antibodies raised against phosphorylated α-synuclein.

Peripheral nervous system

To analyze LBAS of the peripheral nerve, tissue sections from epicardium and epicardial fat of the left ventricle of the heart, sympathetic ganglia, esophagogastric mucosal junction, adrenal gland[22] and abdominal skin[26] were examined by using antibodies raised against phosphorylated α-synuclein.

Olfactory mucosa

At the time of autopsy, the olfactory mucosa, bony septae and contiguous cribriform plate were removed en bloc (Fig. 1). The cribriform plate was dissected in the sagittal plane of the midline by using an electric jigsaw. The left side was fixed for 24 h in 4% paraformaldehyde. After fixation, the olfactory mucosa was removed, dehydrated in a graded alcohol series, cleared in xylene and embedded in paraffin. The right side was fixed for 24 h in 4% paraformaldehyde, decalcified with EDTA for 2 weeks, and dehydrated and embedded in paraffin. Serial 6-μm-thick sections were stained with HE and immunolabeled with antibodies against phosphorylated α-synuclein, PGP9.5, phosphorylated neurofilament, tyrosine hydroxylase, phosphorylated tau and amyloid β (Table 1). In particular, the olfactory receptor neurons of the olfactory epithelium were identified by using PGP9.5 immunohistochemistry.[19] The normal anatomical appearance of the olfactory system is shown in Figure 2.

Olfactory bulb

The olfactory bulbs were prepared for histologic sections to analyze the presence of LBAS. By using HE stain and α-synuclein antibodies, LBAS were identified in the glomeruli, mitral cells, tufted cells and granular cells as previously reported.[11] Mitral and tufted cells were distinguished by their specific shapes. Each neuron was identified when it had an apparent nucleus containing a prominent nucleolus and Nissl substance.

Semiquantitative scoring system of Lewy-related pathology

For each section, we semi-quantitatively graded the immunohistochemical staining with antibody raised against phosphorylated α-synuclein. Our grading system was modified based on the scoring system of the third report of the DLB consortium[34] because we used both the HE stain and immunohistochemistry using monoclonal antibody for phosphorylated α-synuclein to identify LBAS.

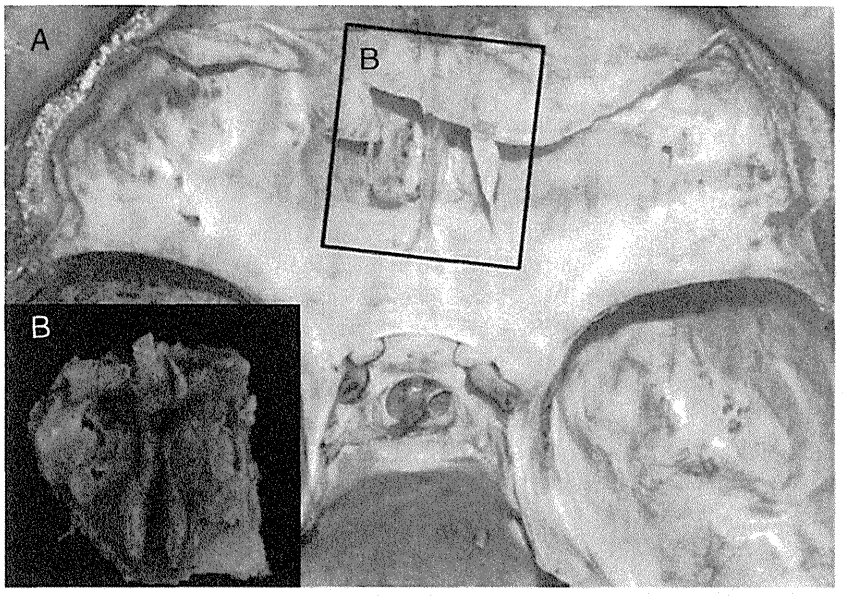

Fig. 1 (a) The anterior cranial fossa after removal of the brain. In order to obtain the olfactory mucosa, the bony septae and contiguous cribriform plate (the rectangular area) were dissected using an electric jigsaw. (b) An inset shows the olfactory mucosa and cribriform plate from the opposite side of the rectangular area.

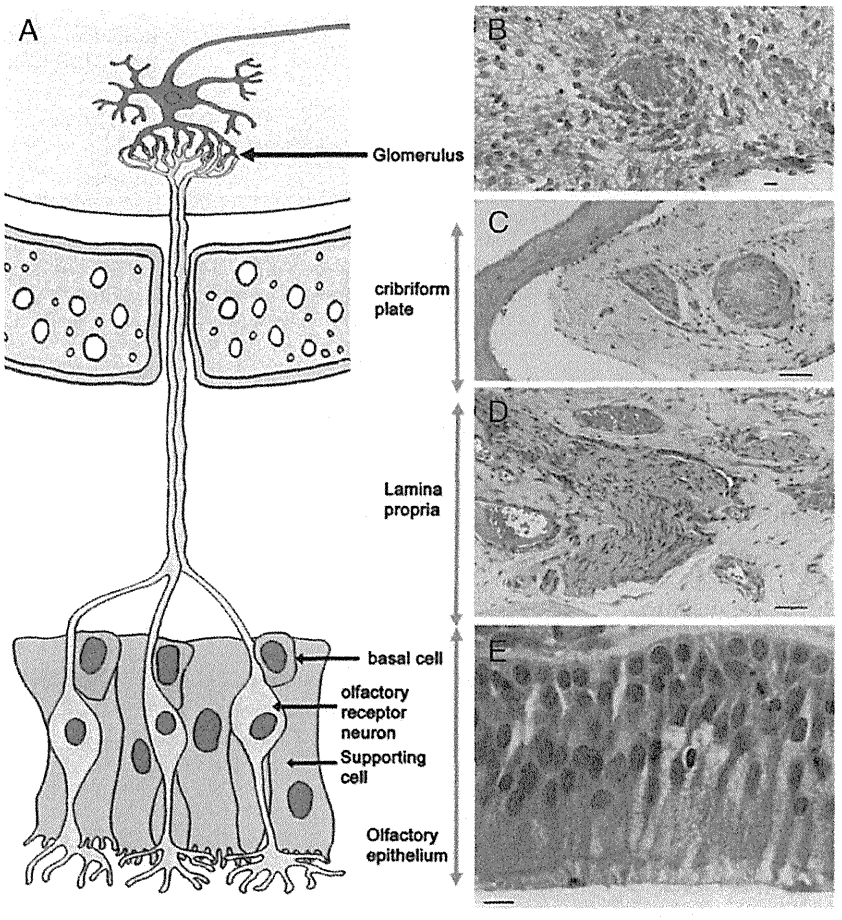

Fig. 2 Scheme of the normal olfactory pathway (a) and photomicrographs of representative histologies of each region (b–e). The olfactory epithelium is composed of three cell types: the basal cells, olfactory receptor neurons and supporting cells (a). The basal cells are the progenitor of the olfactory receptor neurons (a, e). In general, the turnover rate of the olfactory receptor neurons is approximately 30–90 days. Nerve fibers are present in the lamina propria and cribriform plate (c and d, respectively). They consist of either the axons of the olfactory receptor neurons or postganglionic sympathetic nerve fibers. There are glomeruli in the olfactory bulb (b). Glomeruli are the synaptically connected structures of the axons of the olfactory receptor neurons and mitral/tufted cells in the olfactory bulb. (b, e), scale bar = 10 μm; (c), scale bar = 50 μm; (d), scale bar = 100 μm.